LETTERS
PUBLISHED ONLINE: 15 DECEMBER 2014 | DOI: 10.1038/NPHYS3183
nature physics

Increasing the elastic modulus of graphene by controlled defect creation

Guillermo López-Polín[1], Cristina Gómez-Navarro[1,2*], Vincenzo Parente[3], Francisco Guinea[3], Mikhail I. Katsnelson[4], Francesc Pérez-Murano[5] and Julio Gómez-Herrero[1,2]

The extraordinary strength, stiffness[1] and lightness of graphene have generated great expectations of its application in flexible electronics and as a mechanical reinforcement agent. However, the presence of lattice defects, unavoidable in sheets obtained by scalable routes, might degrade its mechanical properties[2,3]. Here we report a systematic study on the elastic modulus and strength of graphene with a controlled density of defects. Counter-intuitively, the in-plane Young's modulus increases with increasing defect density up to almost twice the initial value for a vacancy content of ∼0.2%. For a higher density of vacancies, the elastic modulus decreases with defect inclusions. The initial increase in Young's modulus is explained in terms of a dependence of the elastic coefficients on the momentum of flexural modes predicted for two-dimensional membranes[4,5]. In contrast, the fracture strength decreases with defect density according to standard fracture continuum models. These quantitative structure–property relationships, measured in atmospheric conditions, are of fundamental and technological relevance and provide guidance for applications in which graphene mechanics represents a disruptive improvement.

Modifying the strength and stiffness of 3D conventional materials by defect inclusion is a well-established technique in mechanical engineering. Reducing the dimensionality of the material usually entails an increase in the influence of defects. Furthermore, sometimes reduced dimensionality creates new emergent phenomena that have also to be considered. Graphene, a true 2D crystalline membrane of covalently bonded carbon atoms, has been shown to exhibit an extraordinary intrinsic in-plane strength and Young's modulus[1], close to the elastic constant of the carbon covalent bonds. Experimental findings reveal a strong dependence of the mechanical properties on the defect content. A paradigmatic example is graphene derived from chemical reduction of graphene oxide, which, owing to its partially amorphous character, exhibits an elastic modulus five times smaller than that of pristine graphene[2]. For polycrystalline graphene produced by chemical vapour deposition the effects of sample processing details in the grain boundaries significantly alter the elastic constants and strength of the sheets[3,6,7]. Unfortunately, the fact that these defect contents are not controlled, but rather imposed by synthesis procedures and growth dynamics, hinders systematic studies. A comprehensive approach to the role of disorder in graphene requires the introduction of defects in a controlled manner.

Therefore, to establish reliable structure–properties relationships the natural strategy is to begin with a pristine graphene sheet obtained by micro-exfoliation, for subsequent introduction of a known quantity of defects. Vacancies of carbon atoms are the simplest and most studied type of defect in graphene. Recently, several theoretical works, performed using different approaches[8–10], have predicted a decrease of both the 2D elastic modulus (E_{2D}) and strength with the introduction of such a type of defect, as intuition would dictate. As we shall demonstrate, these calculations and naive expectations fail. Herein we present clear experimental evidence supporting that in graphene the value E_{2D} can be significantly increased by the inclusion of a low density of defects in its atomic structure. We attribute this effect to suppression of the out-of-plane fluctuations by defects[11].

For this study graphene drumheads were prepared by mechanical exfoliation of natural graphite on Si(300 nm)/SiO_2 substrates with predefined circular wells with diameters ranging from 0.5 to 3 μm (Supplementary Information 1). The mechanical properties of the membranes were subsequently tested by indenting with an atomic force microscopy (AFM) tip at the centre of the suspended area (details about the AFM probe can be found in Supplementary Information 2). AFM indentation experiments on graphene drumheads (Fig. 1) can be modelled as clamped circular membranes with central point loading (Supplementary Information 4). The force versus indentation curves can be approximated by the Schwering-type solution as equation (1) (refs 1,12).

$$F(\delta) = \pi\sigma_0\delta + \frac{E_{2D}}{a^2}\delta^3 \quad (1)$$

where F is the loading force, δ is the indentation at the central point, σ_0 is the pre-tension accumulated in the sheet during the preparation procedure and a is the drumhead radius (Methods). Results obtained in up to 30 pristine drumheads yielded values of E_{2D} in the range 250–360 N m^{-1} (Supplementary Information 4) and σ_0 ranging from 0.05 to 0.8 N m^{-1}, with no correlation between pre-stress and E_{2D} (Supplementary Fig. 8).

The fracture strength of the membranes was measured by loading some drumheads up to the failure point. The measured breaking forces (F_{max}) were ∼1.7–2.1 μN. Considering that the maximum stress under the tip can be expressed as $\sigma = (F_{max}E_{2D}/4\pi R_{tip})^{1/2}$, we obtain values of the breaking strength between 28 and 35 N m^{-1}. Summarizing, our elastic and strength values for pristine graphene are compatible with those reported previously in the literature[1,13,14] (Supplementary Information 11).

With the aim of introducing a controlled density of defects, the samples were irradiated with a known dose of Ar^+ with an energy of 140 eV (see Methods and Supplementary Information 5).

[1]Departamento de Física de la Materia Condensada, Universidad Autónoma de Madrid, 28049 Madrid, Spain. [2]Centro de Investigación de Física de la Materia Condensada, Universidad Autónoma de Madrid, 28049 Madrid, Spain. [3]Instituto de Ciencia de Materiales, CSIC, 28049 Madrid, Spain. [4]Radboud University Nijmegen, Institute for Molecules and Materials, Heyendaalseweg 135, NL-6525AJ Nijmegen, The Netherlands. [5]Instituto de Microelectrónica de Barcelona, CSIC, 08193 Bellaterra, Spain. *e-mail: cristina.gomez@uam.es

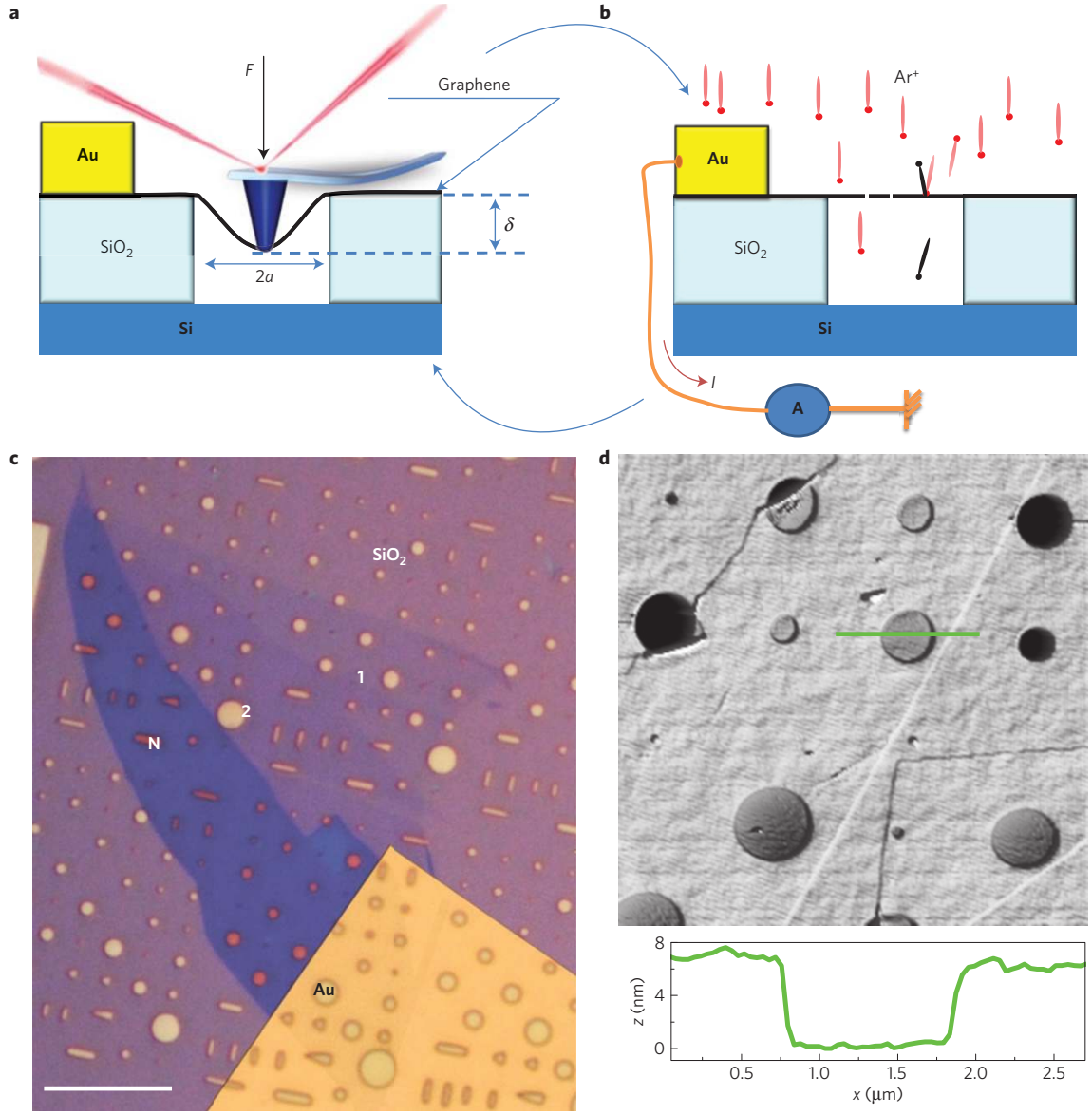

Figure 1 | Set-up and sample geometry. a, Device geometry and scheme of the nanoindentation set-up, which uses an AFM tip for mechanical testing of the suspended graphene layer. **b**, Irradiation set-up, where the defects induced by the incoming argon ions (red) were monitored *in situ* by measuring the ionic current density. The current, *I*, is measured with an ammeter. **c**, Optical microscopy image of a mono-(1), bi-(2) and multi-layer (N) graphene contacted by a gold electrode deposited on an array of wells. Scale bar, 15 μm. **d**, AFM image (top view) of a graphene sheet covering several circular wells. The graph corresponds to the topographic profile along the green line in the image.

In these conditions a random spatial distribution of both mono- and di-vacancies of carbon atoms in a 3:1 ratio is created[15,16]. The nature and density of defects were tested by Raman spectroscopy and scanning tunnelling microscopy (STM). Figure 2a shows a representative STM image (acquired in atmospheric conditions) of a graphite sample irradiated in the same conditions as graphene flakes (see Supplementary Information 7 for further details). The threefold perturbation observed at the centre of the image identifies it unambiguously as an atomic point defect; characterization of suspended graphene membranes by Raman spectroscopy reveals the in-plane (sp^2) character of the defects. These two experimental findings together point towards either pure carbon vacancies or, most likely, vacancies chemically saturated by small atoms. STM imaging of the surface for periods of several days showed no trace of image degradation due to adsorption of airborne molecules.

Mechanical testing was performed after each irradiation dose with the same AFM probe and in the same conditions as described above. Irradiated samples showed a similar F versus δ dependence to the non-irradiated ones. Figure 2b–d gathers representative data for a pristine drumhead (as deposited) and the same drumhead irradiated with a dose of 4×10^{12} defects cm^{-2}, corresponding to a mean defect distance of 5 nm. The defect-free membrane shows an E_{2D} of 305 N m^{-1}, whereas the one with defects shows a higher E_{2D} (484 N m^{-1}). Figure 2d characterizes the measurements from a statistical viewpoint: the distance between the maxima of the Gaussians is about ten times their width.

In view of the above results we went on to irradiate the samples in smaller steps. Dark and light green circles in Fig. 3a depict the results obtained for two representative drumheads, which were characterized after each irradiation dose. Our main experimental finding is that the E_{2D} of the graphene membrane increases with increasing irradiation dose and reaches a maximum of 550 N m^{-1} at a mean distance between defects of ~5 nm (0.2% defect content). For a higher defect content we observe a decreasing E_{2D}. Figure 3a

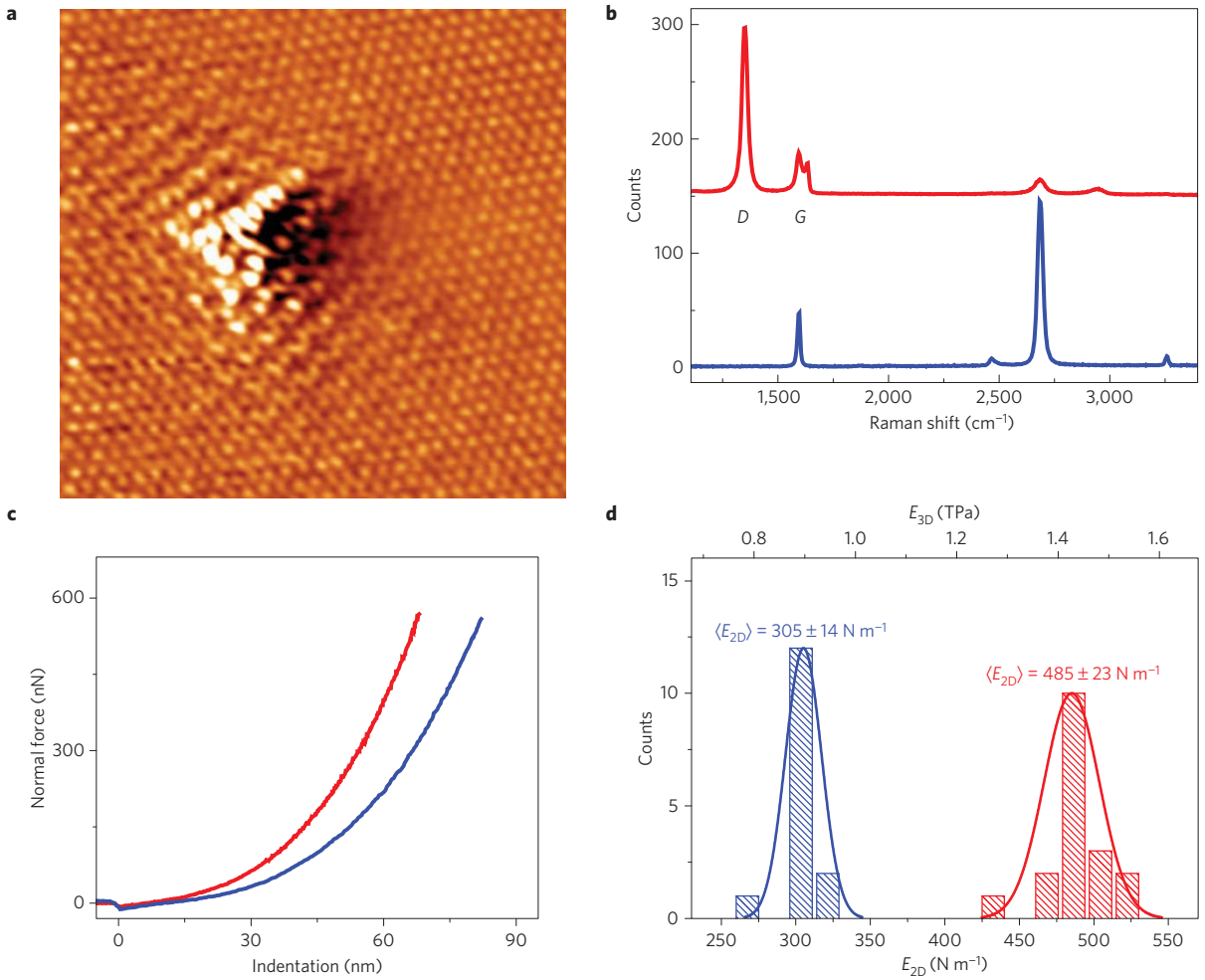

Figure 2 | Characterization of pristine and defective graphene. a, STM image acquired in air at room temperature of a defect created on a graphite sample irradiated under the same conditions as described in the main text. The image is in excellent agreement with those reported previously for single atomic vacancies[17]. The electronic perturbation near the defects, observed as a threefold periodicity surrounding the defect, identifies it unambiguously as a point defect. **b**, Raman spectra of the same membrane before (blue) and after (red) irradiation. The post-irradiation curve is shifted vertically for clarity. The defect density was estimated from the intensity relation between the *D* and *G* peaks. **c**, $F(\delta)$ obtained in the same drumhead before (blue) and after (red) irradiation. **d**, Histogram of E_{2D} obtained from several indentations in the same drumhead before (blue) and after (red) irradiation. To facilitate a comparison with three-dimensional materials, on the upper axis we divide the results by the interatomic layer spacing in graphite (0.34 nm). In **b**–**d** irradiation yields 4×10^{12} defects cm^{-2}.

presents a low data dispersion with a distinct and robust tendency. The pre-tensions in irradiated membranes undergo a slight increase, but they are always below 0.8 N m^{-1} (Supplementary Fig. 8), which following previous reports[1] and detailed studies in our group (to be published elsewhere) do not by themselves justify the observed variations of E_{2D}.

With the aim of understanding the transition between pristine graphene and graphene oxide, a recent work[14] studied the dependence of Young's modulus in graphene as a function of oxygen plasma time. Although at first sight the monotonic drop of elastic modulus with oxygen-created defects looks contradictory to our findings, detailed comparison points towards compatibility of the two experimental observations (see Supplementary Information 16 for further details). As the oxygen plasma simultaneously produces several types of defects, a direct comparison of both sets of results can be made only at very low defect densities, where the data are not contradictory. The region of defect densities where we observe the maximum in E_{2D} is indeed not sampled in ref. 14 (Supplementary Information 16). Furthermore, the appearance of large multi-vacancies in samples subjected to short periods of oxygen plasma justifies a pronounced drop in the elastic modulus that should counteract our observed increase of E_{2D}.

Although there is no complete agreement in the theoretical predictions[17,18], most studies, performed either by molecular dynamics or density functional theory, do not predict an increase in the elastic modulus with such a dilute density of defects[8,9,19], but rather a loss of rigidity (Supplementary Information 12). None of these works considered the influence of defects in graphene within the framework of the thermodynamic theory of crystalline membranes[5,11,20] (Supplementary Information 9). Graphene exhibits a very low bending rigidity (κ) of $\sim$1 eV, comparable to that measured in biological membranes, where it is well known that entropic effects renormalize the elastic constants. The low κ introduces significant temperature (T) fluctuations and strong anharmonic effects, which are important for wavevectors such as $q \ll q^* < \sqrt{(k_B T E_{2D})/\kappa^2}$, with a corresponding Ginzburg length[21] ($\lambda^* = 2\pi/q^*$) at $T = 300$ K of the order of few nanometres. Anharmonicity is reflected in strong coupling between in-plane and out-of-plane fluctuations, giving rise to an exotic elasticity of the membrane, including the absence of any finite elastic constants in the thermodynamic limit, a negative Poisson's ratio, and

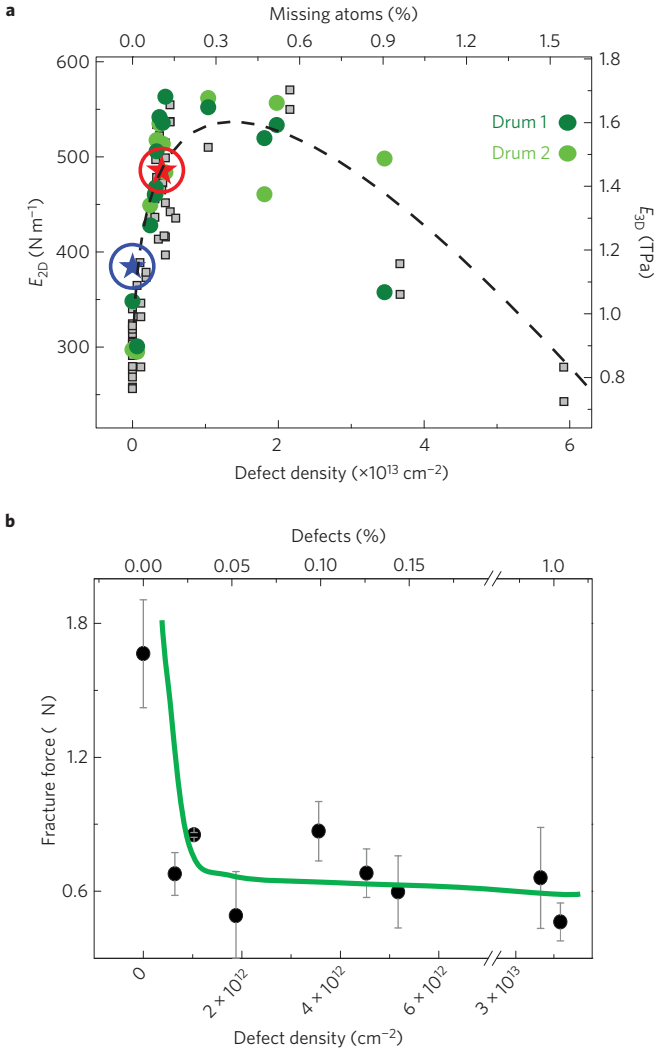

Figure 3 | Mechanical characterization as a function of defect density. **a**, E_{2D} as a function of defect concentration. Dark and light green circles correspond to two representative drumheads (drum 1 and drum 2) that were tracked after multiple irradiations. Grey squares represent measurements of up to 20 different drumheads contained in five different membranes. Blue and red circled stars correspond to the values of E_{2D} obtained from the measurements depicted in Fig. 2. Error bars are not shown for the sake of clarity. Measurements with errors bars can be found in Supplementary Information 4. The dashed line is a fit to equation (2) in the main text. **b**, Breaking force for multiple drumheads as a function of the defect density created . Error bars correspond to the standard deviation of measurements performed on different drumheads. The green line is a guide to the eye.

thermal fluctuations characterized by a large anomalous dimension and negative thermal expansion. In particular, anharmonicity also introduces a wavevector-dependent elastic modulus, $E_{2D} \propto q^{\eta_u}$, where $\eta \sim 0.36$ and q is the momentum or inverse length of flexural phonons[4]. This dependence can be understood as a partial screening of the elastic coefficients due to the contribution from out-of-plane fluctuations to the free energy of the membrane (Supplementary Information 9). Long-wavelength excitations are favoured in large and clean samples, where flexural modes have a long mean free path. According to our estimates (Supplementary Information 9 and 10), defects lower the mean free path of flexural phonons, eventually leading to their localization when $2\pi q^{-1} \sim d$, where d is the mean distance between vacancies. As illustrated in Fig. 4, the presence of

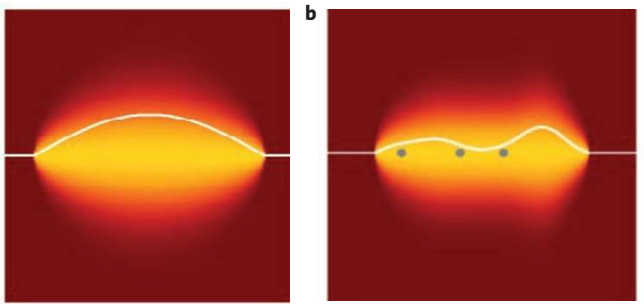

Figure 4 | Thermal fluctuation in 2D membranes. a, Schematic picture of the fluctuations of a suspended graphene membrane. **b**, In the presence of defects, long-wavelength fluctuations are quenched.

defects suppresses flexural modes with longer wavelengths that do not contribute to the decrease of E_{2D}, leading to an effective increase (Supplementary Information 14 and 15). Note that we cannot discard a related scenario involving quenched ripples in suspended samples, as observed in TEM images under electron irradiation[22]. Further support for our interpretation stems from our experimental observation that pristine membranes exhibit enhanced E_{2D} with increasing induced pre-stress (to be published), as predicted by the suppression of anharmonic effects in stiff membranes[23].

This growth in the elastic coefficients would compete with the predicted softening effect of vacancies[8,10,19] and would be suppressed as the vacancy concentration approaches the percolation threshold, where the elastic coefficients are expected to decrease linearly with the number of vacancies and would be proportional to the initial value of the coefficients. Taking into account these two competing mechanisms, we can write a qualitative expression as:

$$E = K\left(b + \frac{1}{l_0^2} + n_i\right)^{\eta/2}\left(1 - c\left(\frac{1}{l_0^2} + n_i\right)\right) \qquad (2)$$

where K and c are constants, b is a geometrical factor of the order of the inverse of the area of the drumhead that accounts for boundary conditions, l_0 is the localization length for flexural phonons in pristine graphene and n_i is the density of defects induced by irradiation. The dashed line in Fig. 3a depicts a fitting to our experimental results according to equation (2). Best fitting to our experimental data yields $K = 1.5 \times 10^9$ N m$^{\eta-2}$, $l_0 = 70$ nm, $\eta = 0.36$ and $c = 1.2 \times 10^{-18}$ m^2. As $1/l_0^2$ is much greater than b ($\sim 1/a^2$, with a being the hole radius) it can be neglected in the equation. From the fit we can conclude that the initial E_{2D} in our samples is mainly dictated by the effective scattering length $l_0 \sim 10$–100 nm. This value is smaller than that reported for the localization length of flexural modes[21] at temperatures above 100 °C; we attribute this difference to physisorption on our samples that desorbs at temperatures above 70 °C. This low value of l_0 does not allow experimental observation of the predicted dependence on the drumhead area. Our fitting value for the constant c is higher than that predicted by molecular dynamics[10,19]; this discrepancy can be attributed to defect agglomeration that might take place only at our higher irradiation doses, as reported in ref. 24. Furthermore, vacancies lead to resonances at the Dirac energy and to the formation of a vacancy band with a high density of states; the formation of such states results in a decrease in the elastic modulus[25].

Interestingly, the average distance between defects at maximum E_{2D} is about 5 nm (Fig. 3a), which coincides fairly well with the above-mentioned Ginzburg length beyond which flexural modes cease to be anharmonic. Hence, modes with shorter wavelengths do not screen the elastic constants.

Our findings imply that the applicability of atomistic models to mesoscopic membranes[26] might not be straightforward

(see Supplementary Information 12 and 13 for a detailed discussion). In our experiments the variation of Young's modulus takes place at relatively large vacancy distances (4–20 nm). Hence well-averaged calculations should involve large slabs with more than 10,000 atoms. Although these sizes can be reached with molecular dynamic simulations, the results will always depend on the accuracy of the selected potential. Precise DFT calculations beyond perturbation theory, fully including thermal fluctuations of flexural phonons, electron–phonon coupling and atom slabs as large as possible, should address our observations.

Note also that our proposal, together with the experimental data, implies a non-renormalized $E_{2D} > 550\,N\,m^{-1}$. Experimental data on pre-strained graphene membranes (to be published) yield even higher values—that is, $\sim 700\,N\,m^{-1}$. The lower E_{2D} measured by nanoindentation in irradiated samples versus those obtained in pressurized membranes[23] suggests that defects do not totally cancel the entropic effects.

Finally, measurements of the breaking force showed a markedly different behaviour when compared to E_{2D}. The fracture force of irradiated membranes exhibits a pronounced decrease with increasing defect density, as depicted in Fig. 3b. The measured failure forces drop by a factor of two for the lower irradiation dose, corresponding to a mean distance between defects of 12 nm. This corresponds to a 30% reduction in strength (see Supplementary Information 11). For higher defect densities the value of the breaking force shows a high dispersion, varying from 400 to 800 nN. We observe no further significant drop, even for irradiation doses as high as 4×10^{13} defects cm^{-2} ($\sim$1%), indicating a saturation tendency. In contrast to the behaviour of E_{2D} with defect density, which cannot be explained by conventional continuum mechanics, the fracture strength dependence can be addressed by classical models[9].

Our determination of the relevance of defects to the mechanical properties of suspended graphene sheets raises fundamental issues in 2D materials that can be extrapolated to other atomic thin membranes, such as BN and MoS_2. The elasticity and strength versus defect concentration relationships provided, measured in ambient conditions, open new paths to tailoring the stiffness of future graphene-based devices. The introduction of such amounts of defects should enhance the sensitivity of mass sensors based on graphene resonators and should be taken into account when using graphene as a reinforcement agent.

Methods

Figure 1 shows the sample geometry. Single layers of graphite were found by optical microscopy and corroborated by Raman spectroscopy[27] (Supplementary Information). Non-contact AFM images of the drumheads showed that graphene layers adhere to the vertical walls of the wells to a depth of 2–10 nm (Fig. 1d). The experiments described in this work were carried out in ambient conditions. Only membranes showing a flat and featureless surface (that is, absence of bubbles or wrinkles) and no noticeable slack were selected for the measurements. Repeated loading/unloading cycles on the same membrane (see Supplementary Information 3) showed high reproducibility, completely reversible behaviour and no signature of fatigue.

Obtaining E_{2D} from equation (1) requires a precise determination of the tip–membrane contact point, which is not always easy to determine from experimental curves. To check the robustness and validity of indentation curves we have used three different equations to fit the indentation curves (see Supplementary Information 4 for detailed information). Differences between these fittings are within 20% in absolute value, but always yield a similar tendency. For the values reported here, E_{2D} was estimated from the coefficient in δ^3 of a complete third-order polynomial (mode 3 described in Supplementary Information 4).

The density of defects was estimated by two independent methods: *in situ* by measuring the ionic current density as a function of time and *ex situ* by performing Raman spectroscopy after each irradiation dose. The mean distance between defects was deduced from the intensity relation between the *D* and *G* peaks in the Raman spectra[24,28]. Both methods yield similar results. Raman spectroscopy[29] and STM characterization at the atomic level (see Fig. 2a and Supplementary Information 6 and 7) also corroborated the vacancy-like character of the induced defects, ruling out out-of-plane chemisorption in air. AFM images of the drumheads and surrounding regions after irradiation showed no differences from those of images before irradiation. We have not observed signatures of plasticity (that is, irreversible effects) up to the forces reached in our indentations.

Our results are robust with respect to tip variations. We measured with different probes, always finding the same tendency and similar values to those shown in Fig. 3a. Consecutive indentations with the same tip in alternating pristine and irradiated samples yielded consistent E_{2D} enhancement in the irradiated samples. The analysis described in Supplementary Information 4 is accurate for indentation curves with maximum forces above 200 nN. This threshold is much smaller than the maximum force used for pristine (800 nN) and irradiated (600 nN) samples.

Received 24 June 2014; accepted 10 November 2014; published online 15 December 2014

References

1. Lee, C., Wei, X. D., Kysar, J. W. & Hone, J. Measurement of the elastic properties and intrinsic strength of monolayer graphene. *Science* **321,** 385–388 (2008).
2. Gomez-Navarro, C., Burghard, M. & Kern, K. Elastic properties of chemically derived single graphene sheets. *Nano Lett.* **8,** 2045–2049 (2008).
3. Lee, G-H. *et al.* High-strength chemical-vapor-deposited graphene and grain boundaries. *Science* **340,** 1073–1076 (2013).
4. Aronovitz, J. A. & Lubensky, T. C. Fluctuations of solid membranes. *Phys. Rev. Lett.* **60,** 2634–2637 (1988).
5. Nelson, D., Piran, T. & Weinberg, S. (eds) *Statistical Mechanics of Membranes and Surfaces* 2nd edn (World Scientific Singapore, 2004).
6. Huang, P. Y. *et al.* Grains and grain boundaries in single-layer graphene atomic patchwork quilts. *Nature* **469,** 389–392 (2011).
7. Ruiz-Vargas, C. S. *et al.* Softened elastic response and unzipping in chemical vapor deposition graphene membranes. *Nano Lett.* **11,** 2259–2263 (2011).
8. Fedorov, A. S. *et al.* DFT investigation of the influence of ordered vacancies on elastic and magnetic properties of graphene and graphene-like SiC and BN structures. *Phys. Status Solidi B* **249,** 2549–2552 (2012).
9. Georgantzinos, S. K., Katsareas, D. E. & Anifantis, N. K. Limit load analysis of graphene with pinhole defects: A nonlinear structural mechanics approach. *Int. J. Mech. Sci.* **55,** 85–94 (2012).
10. Jing, N. *et al.* Effect of defects on Young's modulus of graphene sheets: A molecular dynamics simulation. *Rsc Adv.* **2,** 9124–9129 (2012).
11. Katsnelson, M. I. & Fasolino, A. Graphene as a prototype crystalline membrane. *Acc. Chem. Res.* **46,** 97–105 (2013).
12. Begley, M. R. & Mackin, T. J. Spherical indentation of freestanding circular thin films in the membrane regime. *J. Mech. Phys. Solids* **52,** 2005–2023 (2004).
13. Bunch, J. S. *et al.* Electromechanical resonators from graphene sheets. *Science* **315,** 490–493 (2007).
14. Zandiatashbar, A. *et al.* Effect of defects on the intrinsic strength and stiffness of graphene. *Nature Commun.* **5,** 3186 (2014).
15. Krasheninnikov, A. V. & Banhart, F. Engineering of nanostructured carbon materials with electron or ion beams. *Nature Mater.* **6,** 723–733 (2007).
16. Ugeda, M. M., Brihuega, I., Guinea, F. & Gomez-Rodriguez, J. M. Missing atom as a source of carbon magnetism. *Phys. Rev. Lett.* **104,** 096804 (2010).
17. Guryel, S. *et al.* Effect of structural defects and chemical functionalisation on the intrinsic mechanical properties of graphene. *Phys. Chem. Chem. Phys.* **15,** 659–665 (2013).
18. Kvashnin, A. G., Sorokin, D. G. & Kvashnin, D. G. The theoretical study of mechanical properties of graphene membranes. *Fullerenes Nanotubes Carbon Nanostruct.* **18,** 497–500 (2010).
19. Neek-Amal, M. & Peeters, F. M. Linear reduction of stiffness and vibration frequencies in defected circular monolayer graphene. *Phys. Rev. B* **81,** 235437 (2010).
20. Katsnelson, M. I. *Graphene: Carbon in Two Dimensions* (Cambridge Univ. Press, 2012).
21. Ghosh, S. *et al.* Extremely high thermal conductivity of graphene: Prospects for thermal management applications in nanoelectronic circuits. *Appl. Phys. Lett.* **92,** 151911 (2008).
22. Meyer, J. C. *et al.* The structure of suspended graphene sheets. *Nature* **446,** 60–63 (2007).
23. Roldan, R., Fasolino, A., Zakharchenko, K. V. & Katsnelson, M. I. Suppression of anharmonicities in crystalline membranes by external strain. *Phys. Rev. B* **83,** 174104 (2011).
24. Lucchese, M. M. *et al.* Quantifying ion-induced defects and Raman relaxation length in graphene. *Carbon* **48,** 1592–1597 (2010).

25. Vaks, V. G., Katsnelson, M. I., Likhtenstein, A. I., Peschanskikh, G. V. & Trefilov, A. V. Pretransition softening and anomalous pressure-dependence of shear constants in alkali and alkaline-earth metals due to band-structure effects. *J. Phys. Condens. Matter* **3,** 1409–1428 (1991).
26. Leenaerts, O., Peelaers, H., Hernandez-Nieves, A. D., Partoens, B. & Peeters, F. M. First-principles investigation of graphene fluoride and graphane. *Phys. Rev. B* **82,** 195436 (2010).
27. Ferrari, A. C. *et al.* Raman spectrum of graphene and graphene layers. *Phys. Rev. Lett.* **97,** 187401 (2006).
28. Cancado, L. G. *et al.* Quantifying defects in graphene via Raman sectroscopy at different excitation energies. *Nano Lett.* **11,** 3190–3196 (2011).
29. Eckman, A. *et al.* Probing the nature of defects in graphene by Raman spectroscopy. *Nano Lett.* **12,** 3925–3930 (2012).

Acknowledgements

This work was supported by MAT2013-46753-C2-2-P, Consolider CSD2010-0024, FIS2011-23713 and the European Research Council Advanced Grant, #290846.

We acknowledge technical support from A. Aranda, C. Salgado and A. del Campo, and fruitful discussions with M. Jaafar, A. K. Geim, R. Perez, F. Yndurain and J. Soler.

Author contributions

C.G-N. and J.G-H. devised the experiments. G.L-P. performed the experiments. G.L-P., C.G-N. and J.G-H. analysed the data. F.P-M. prepared the substrates. C.G-N. and J.G-H. wrote the manuscript. V.P., M.I.K. and F.G. formulated the theoretical model. All authors participated in discussions.

Additional information

Supplementary information is available in the online version of the paper. Reprints and permissions information is available online at www.nature.com/reprints. Correspondence and requests for materials should be addressed to C.G-N.

Competing financial interests

The authors declare no competing financial interests.